Nano-scale hydrogen-bond network improves the durability of greener cements

Johan Jacobsen[1,2]*, Michelle Santos Rodrigues[3]*, Mark T. F. Telling[4,5], Antonio Ludovico Beraldo[3], Sérgio Francisco Santos[6], Laurence P. Aldridge[7] & Heloisa N. Bordallo[1,2]

[1]The Niels Bohr Institute, University of Copenhagen, DK-2100, Copenhagen, Denmark, [2]European Spallation Source ESS AB P.O Box 176, SE-221 00 Lund, Sweden, [3]School of Agricultural Engineering/FEAGRI, UNICAMP, São Paulo, Brazil, [4]ISIS Facility, Rutherford Appleton Laboratory, Chilton, Oxon, UK OX11 0QX, [5]Department of Materials, University of Oxford, Parks Road, Oxford, UK, [6]Department of Biosystem Engineering, Universidade de São Paulo, São Paulo, Brazil, [7]Institute of Materials & Engineering, ANSTO, PMB 1 Menai, NSW2234, Australia.

More than ever before, the world's increasing need for new infrastructure demands the construction of efficient, sustainable and durable buildings, requiring minimal climate-changing gas-generation in their production. Maintenance-free "greener" building materials made from blended cements have advantages over ordinary Portland cements, as they are cheaper, generate less carbon dioxide and are more durable. The key for the improved performance of blends (which substitute fine amorphous silicates for cement) is related to their resistance to water penetration. The mechanism of this water resistance is of great environmental and economical impact but is not yet understood due to the complexity of the cement's hydration reactions. Using neutron spectroscopy, we studied a blend where cement was replaced by ash from sugar cane residuals originating from agricultural waste. Our findings demonstrate that the development of a distinctive hydrogen bond network at the nano-scale is the key to the performance of these greener materials.

Cementitious materials are the most used materials on Earth. This is certainly not related to their superior quality when compared to other materials, but simply because the main oxides present in cement – CaO, SiO_2, Al_2O_3, Fe_2O_3 – constitute over 90% of the earth's crust. This abundant resource makes cement cheap forming the basis of our modern built infrastructure. New infrastructure needed particularly in the developing world demands such immense capital costs that a recent report on infrastructure by the McKinsey Global Institute[1] was named "Infrastructure productivity: How to save \$1 trillion a year". One method of cost saving is to stop building inadequate structures that need high maintenance. Hence the durability of components that create essentially maintenance free infrastructure is of importance. Ordinary Portland Cement (OPC) can be partially replaced by mineral additions containing amorphous fine grained silica in building materials. Such blended cements have many advantages to OPC as they have superior performance indicated by resistance to water penetration[2–6], are generally more economic, and most importantly they replace cement with binders whose manufacture needs less carbon dioxide generation. This can be significant as about 5% of the total man-made generation of carbon dioxide arises from OPC production[7]. Enhancement to the microstructure and durability of blended concretes is due to both chemical and physical effects. For example, Young and Hansen[8] contrasted the influence of water in calcium silicate hydrates of OPC with that found in blended pastes. The blended pastes were found to have almost no calcium hydroxide present whereas OPC pastes exhibited a substantial amount. This difference was due to the pozzolan (or active form of silica) reacting with the "excess" calcium hydroxide. Bakker[5] suggests that the reason why blended pastes have less permeability is essentially because the pozzolan causes blocking of the capillary pores of the paste. While the particle size of the pozzolan directly influences the mechanical effects related to the packing characteristics of mixtures[9], the closing of the capillary pores is of importance to the properties of the concrete. Hooton[10] reported that while the increased durability of blended cements can be connected to the reduced permeability, he found it impossible to attribute changes in water permeability to changes of pore size only. This conclusion was based on the correlation (and lack of correlation) of the "critical pore radius" (identified by MIP) with the permeability of cement pastes. This implies that another factor, other than simple pore blocking, has to be responsible for the improved performance. As Phair[6] has shown there are other technical candidates to produce "greener cement" than blended OPC including; alkali-activated

cements - sometimes called "Geopolymer"[11], magnesia cements and sulphuoaluminate cements. Each of these has some advantages and disadvantages and it is not clear if there is a large-scale commercial market for these cements. In contrast blended cements have been used commercially. In 2000 Schmidt et al[12] reported that in the USA about 98 million tons of ordinary Portland cement were used while about 10 million tons of blended cement were produced. In Europe at this time significantly larger amounts of the cement blends were used in concrete production. In the last decade there has been a significant increase in the use of blended cement doubtless fueled by both their perceived improvement in durability and the fact that their use lowers the carbon footprint of built infrastructure.

Here we focus on the effects of a mineral addition made from fired sugar cane straw ash (SCSA) obtained from the processing of the agricultural waste[13]. This has been shown to be a good cement replacement when burnt at the right conditions to form a fine material with relatively high amorphous silica content[13,14]. However, it has not yet been verified how this pozzolanic reaction affects the water mobility in mature cement pastes. In the particular case of water in hydrating cement paste, it is widely accepted that the state of water influences its mechanical and transport properties, as well as directly impacting upon the durability of building material structures[15]. Such understanding is the focus of this work, and our results provide original and important information for future utilization of these biomass ashes.

Water dynamics can be investigated using many experimental techniques, such as infrared and Raman spectroscopies[16], and Nuclear Magnetic Resonance. From the structural characterization side, by combining neutron powder diffraction with the Rietveld crystal structure refinement method Hartman and Berliner[17] showed the role of hydrogen bonding in the stabilization of the ettringite structure. In this work, the experimental technique of quasi-elastic neutron scattering (QENS) was deemed the most suitable method since it allows the dynamics, and associated geometric of motion, of protons on very short (pico-second) time scales to be investigated. In the case of bulk water, the potential of QENS has been exploited for many years[18,19]. However, it is now also well established that neutron scattering, and QENS in particular, is a powerful technique that can examine the interactions of the pore water with the C-S-H in cement paste[20–25].

Results

In this paper we used neutron scattering to analyze the motion of water molecules in 28 day old OPC paste (100% of cement) and SCSA paste (80% of cement and 20% of ash burnt at 700°C) samples using the backscattering instrument IRIS located at the ISIS Facility, UK (see SI for details). Two types of neutron scattering experiment were performed: (1) Elastic Incoherent Neutron Scattering (EINS) measurements using the elastic fixed window approach[26], which allows analysis of the structure factor, $S_E(Q, \omega \approx 0)$, as a function of neutron scattering vector, Q, and provides a global view of water dynamics in
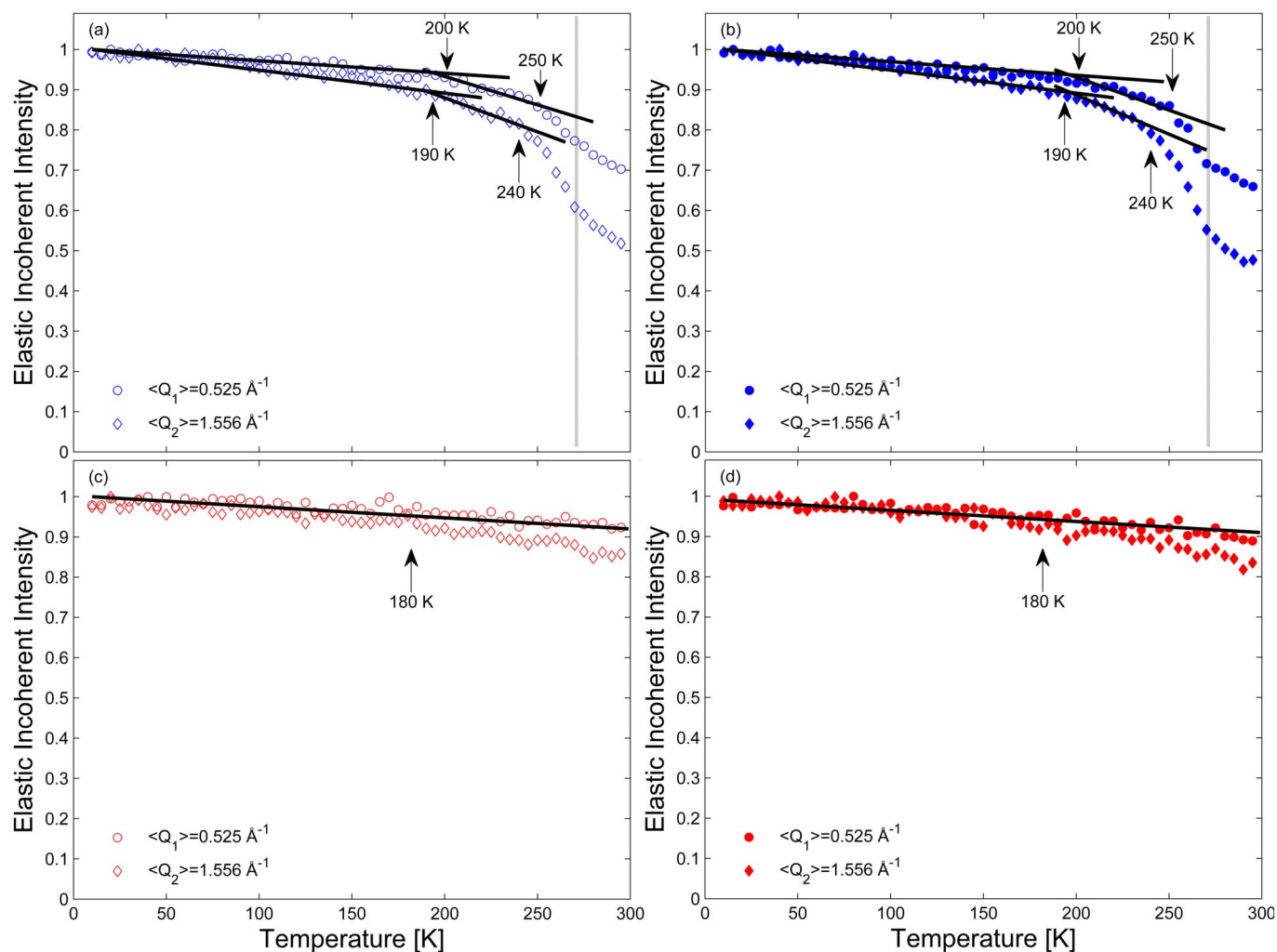

Figure 1 | A comparison between the normalized intensity $S(Q, 0)(T)/S(Q,0)(T = 5 \text{ K})$. (TOP) for the wet and (BOTTOM) dried samples; the arrows mark the temperatures at which an-harmonic onsets occur for OPC (open symbols) and SCSA (full symbols).

the different pastes, and (2) QENS, which gives information on the microscopic motions involved in diffusion of hydrogen containing molecules.

Elastic incoherent neutron scattering evidences diffusive motion. Results obtained from the EINS measurements as a function of temperature, and normalized to the lowest temperature for the hydrated and dried pastes, are presented in Figure 1. As expected the intensity of the elastic line, $S(Q, \omega \approx 0)$, decreases with increasing temperature. However, as indicated by the arrows in Figure 1(a), and in line with other wet cement paste studies[20,21], an anomalous decrease of the elastic intensity occurs at about 190 K and 200 K for scattering vector, $Q = 0.525$ Å^{-1}, and at about 240 and 250 K for $Q = 1.556$ Å^{-1}, respectively. This decrease, seen in both SCSA and OPC, is indicative of the onset of some type of diffusive motion that is faster than the instrumental time resolution ($\sim$150 ps) and thus visible within the resolution of the spectrometer. Moreover, as seen in Figures 1(c,d) for the dried samples a deviation is also observed around 180 K. This behavior is similar to the one reported in clays, and attributed to the activation of OH-motions[27].

The differences in the dynamical transition temperatures as a function of momentum transfer, Q, suggests that for each sample the scattering function is broadening due to the occurrence of a quasi-elastic (QE) signal related to that motional disorder occurring

within the time resolution of experiment; a broadening which is governed by the physical parameters of the individual pore structure. Such a response should give rise to a central narrow elastic peak of approximately the width of the resolution function combined with a broad Lorentzian tail.

Quasi-elastic neutron scattering allows to determine water diffusion coefficients. Indeed, after subtracting the signal due to the paste alone (i.e. a dried sample from which elastic scattering dominates), QE is clearly observed (see SI for details). The analysis of the QE signal enabled us to obtain the correlation times associated with the water mobility in both pastes. Moreover, if the pore size distributions are different we expect different surface-water binding behavior to be evident such that we will consequently discern different relaxation times. In addition, a complete characterization of the geometry of the motion can be obtained by analyzing the relative amplitude of the elastic signal, called the elastic incoherent structure factor (EISF), which provides a measure of the time-averaged spatial distribution of the protons. Finally, it is important to consider that the difference between the lowest values of ratios of $S(Q, \omega \approx 0)$ in Figure 1 can be accounted for by the differences in the ratio of immobile to mobile proton in the samples.

In Figures 2a and 2b we report the normalized quasi-elastic spectra at 300 K, at selected momentum transfer (Q) values, for both
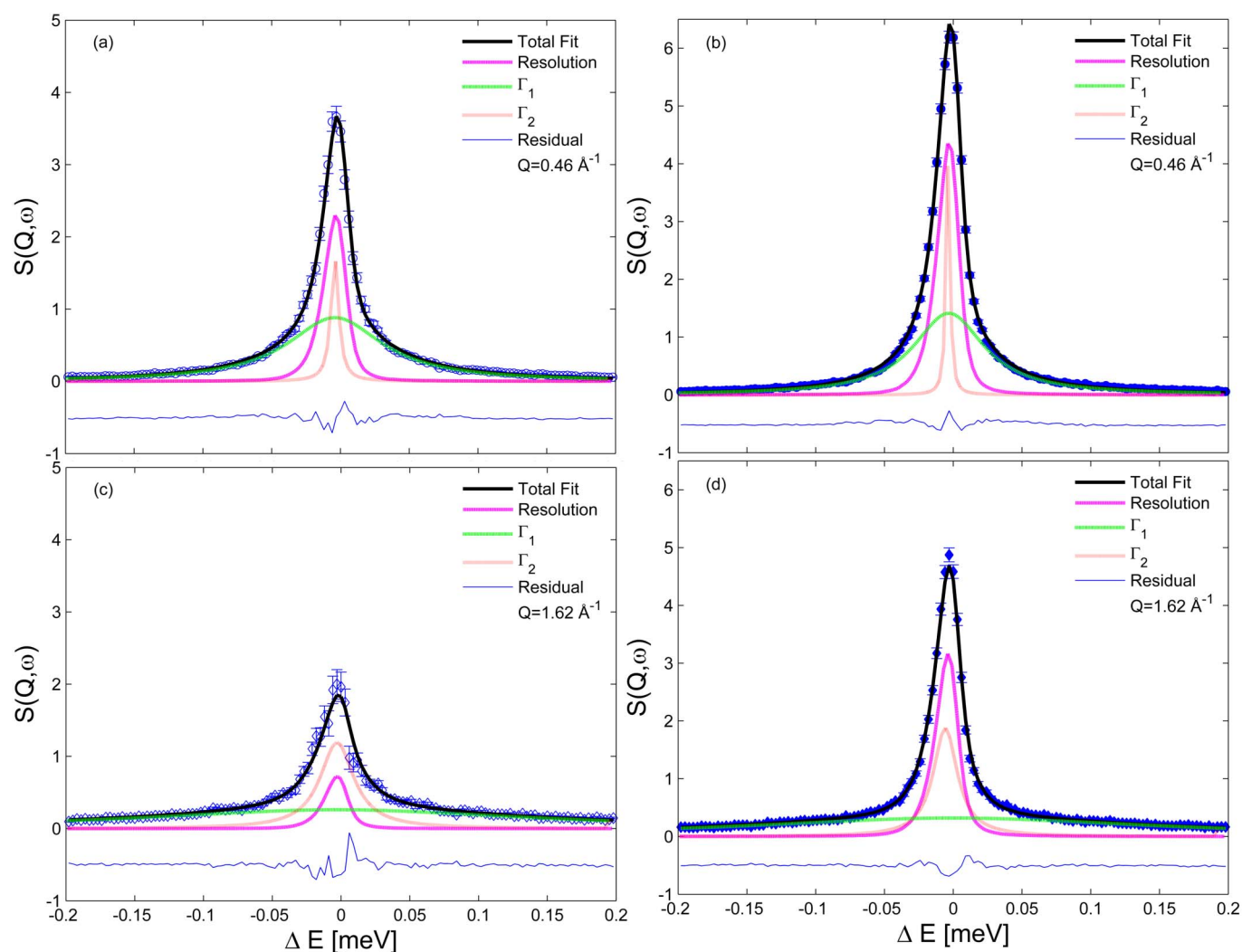

Figure 2 | **Experimental QE spectra at 300 K, for selected Q-values.** For OPC (a, b) and SCSA (c, b), $\Delta E = 17.5$ μeV, together with the best fit (solid line) and the QE components (Γ_1 dotted lines and Γ_2 dash-dot lines). The background is represented in dot lines, and the elastic component in long dashed lines. The residual is also shown.

samples. Initially, the QENS spectra were fitted by means of an elastic peak plus a Lorentzian function using standard least-squares refinement method. Using this phenomenological model we assumed that the chemically "bound" water molecules contribute elastically to the QENS spectra, while the confined water molecules give rise to a QE broadening. For both samples the quality of the fitting procedure was quite poor, therefore an additional QE component was introduced to the phenomenological expression as follows:

$$
\begin{aligned}
S_m(Q,\omega) = F\{&[A_0(Q)\delta(\omega) + A_1(Q)L_1(\Gamma_1,\omega) \\
&+ A_2(Q)L_2(\Gamma_2,\omega)] \otimes F(Q,\omega)\} + B(Q),
\end{aligned}
\tag{1}
$$

where F is a scaling factor, A_i are the structure factors, where $A_0(Q)$ represents the effective EISF, $L_i(\Gamma_i, \omega)$ are the Lorentzian functions having the half-widths at half-maxima (HWHM) Γ_i and $F(Q, \omega)$ is the experimental resolution function. The flat background term,
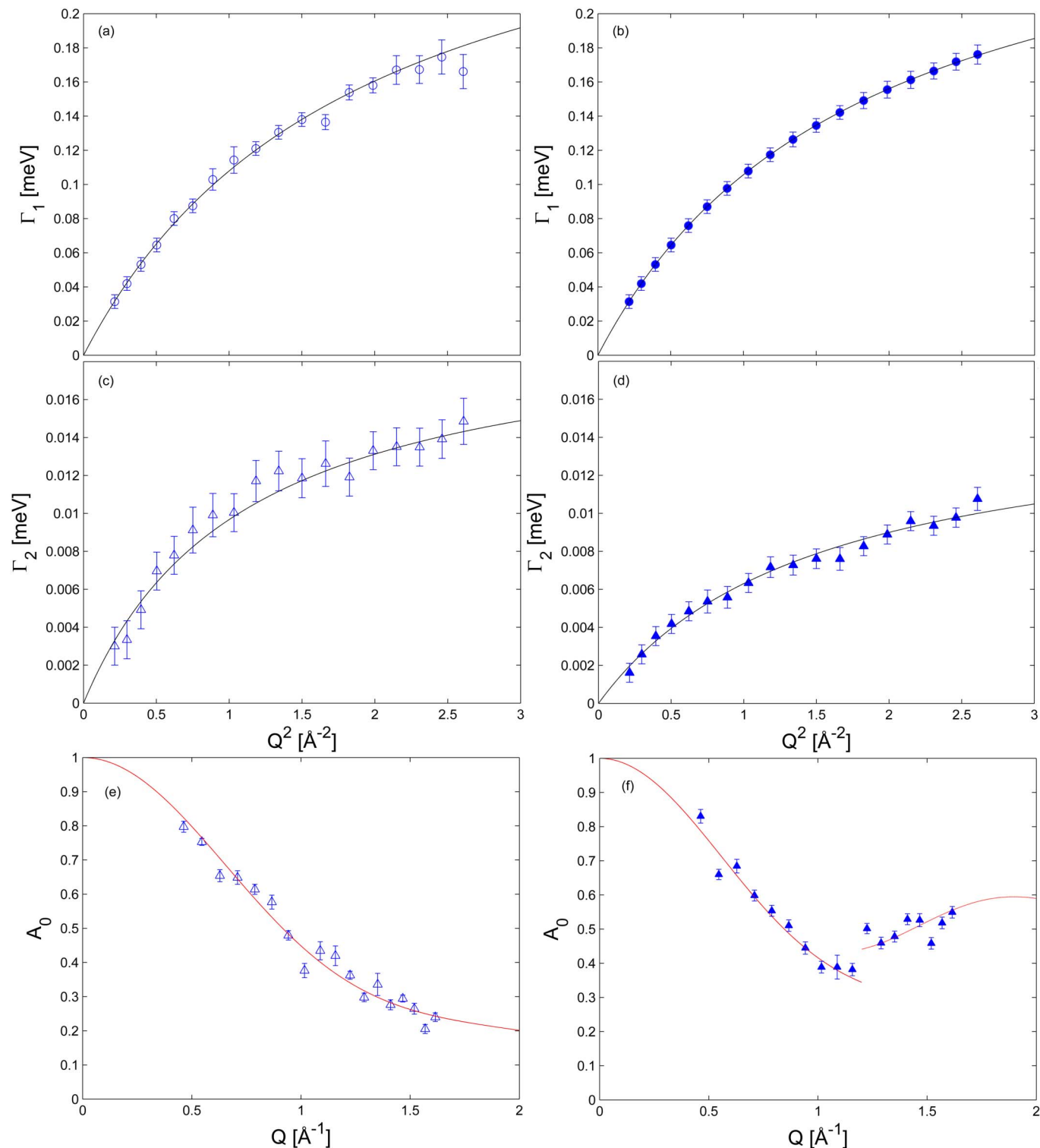

Figure 3 | **Evolution of the HWHM Γ_1 (TOP) and Γ_2 (MIDDLE) vs Q^2 at 300 K; the line is a linear fit using the Singwi and Sjölander model[28] (see text and SI).** For (a) OPC and (b) SCSA. BOTTOM: EISF vs Q obtained from the analysis of quasi-elastic spectra; solid lines were obtained using the models described in the text (see text and SI) for (e) OPC and (f) SCSA.

Table 1 | Parameters characterizing the translational motion of water in the capillary (C) and gel pores (G) for 28 days old OPC and SCSA 300 K, ΔE (FWHM) = 17.5 μeV. Values of bulk water as well as for OPC obtained with energy resolutions of 98 and 30 μeV are given, see Ref. 23 for details

Sample	t_0 (ps)	D_t (10^{-9} m²/s)
Bulk water	1.57 ± 0.12	2.49 ± 0.07
OPC w/c = 0.42[23]	10 ± 1	1.24 ± 0.08 mainly C water
	51 ± 3	0.6 ± 0.1 mainly G water
OPC w/c = 0.45	2.1 ± 0.3	2.5 ± 0.4 for Γ_1
	32.3 ± 0.5	0.28 ± 0.04 for Γ_2
SCSA w/c = 0.45	2.21 ± 0.02	2.49 ± 0.02 for Γ_1
	41.9 ± 0.3	0.16 ± 0.01 for Γ_2

B(Q), that includes quasi-elastic contributions to the spectral intensity arising from fast motion. It should be mentioned that since we are required to model our data using three Lorentzian components, the EISF measured is in fact a global, or effective, EISF for the whole sample rather than a discrete EISF arising from one lone diffusive process.

The broad (Γ_1) and the narrow (Γ_2) Lorentzians can be associated with fast and slow motions of the water molecules, respectively, suggesting that at least two different diffusive-like motions are responsible for the QE signal. Therefore, the variations of Γ vs Q, as depicted in Figures 3(a) and (b), were fitted using the model of Singwi and Sjölander[28].

The obtained values are given in Table 1. It is well known that under confinement water mobility will shift to longer relaxation times with respect to the bulk water processes, while water contained in the large capillary pores behaves "bulk-like". Therefore our results indicate that the fast motion is related to a small percentage of the latter population, while the slower motion is due to the water confined in the smaller gel pores. Moreover, the difference in the values of the diffusion constants obtained for OPC and SCSA is related to differences in the gel pore structure of the pastes; this inner structure playing a major role in governing the mobility of water molecules. The differences between the values previously obtained for the OPC[23] and the ones reported here is a consequence of the different time windows probed by the different spectrometers used. For the work presented here we are probing motions typically in 5–150 ps range. For the previous OPC measurements the time window accessible was sensitive to motions in the 1–10 ps range.

Quasi-elastic neutron scattering affords evidence of evidence different types of hydrogen bounds within the pore structure. This interpretation is further evidenced by the behavior of the effective EISF versus Q in the range 0.5–1.7 Å^{-1} shown in Figures 3(e) and (f), where our results clearly demonstrate the influence of the pozzolan on proton mobility. The first observation is that the effective EISF approaches unity in the limit of low Q, indicating localized dynamics that do not allow the water molecules to diffuse over large distances (which corresponds to low Q values). Secondly, the fact that the effective EISF does not decay to zero for large Q-values indicates an immobile fraction of H-atoms in the examined time-space window, in agreement with the EINS results. Then, in the case of the OPC, the solid line in Figure 3(e) shows that the Volino–Dianoux model[29], where free diffusion in the restricted volume of a sphere is permitted, modified to consider that an immobile fraction of protons, p, are presented in the samples[30], describes well the experimental results for the confined water (see the SI for details). The parameters obtained from this analysis indicate that for the OPC the translational diffusion is confined to a spherical motion with a radius of about 2.7 Å, while in good agreement with the values reported earlier for the ratio of bound to

mobile water in 28 days old hydrated OPC cement[21], the value found here is around 33%. However, for the SCSA sample this model is insufficient to describe the evolution of the effective EISF attributed to the confined molecules over the whole Q-range. Note that after reaching a local minimum around Q = 1 Å^{-1}, the effective EISF increases for higher Q-values indicating that a restricted rotational diffusion takes place. Therefore the effective EISF for the SCSA was divided into two parts. For Q < 1 Å^{-1} it was fitted with the same model used for the OPC sample, showing that 27% of the protons is immobile and that the translational diffusion is confined to a radius comparable to the one obtained for the OPC, while for the higher Q-region the 2-site jump diffusion model, which ascribes the probability for each H atom to jump between two separated sites parameterized by a jump distance d, between a pair of neighboring O atoms, to which it remains restricted, was used (see SI for details). The parameters obtained from this analysis indicate that 7% of the protons in the SCSA are bound to the pore structure with a jumping distance between sites around 4.5 Å.

Discussion

Defining which water states we accessed through this experiment is not trivial as the state of water in a C-S-H system is imprecisely defined. For example, hydrogen can be present (1) within the structure of C-S-H (either in the form of H_2O or OH), (2) as water physically adsorbed on the surface of C-S-H phases and (3) as water in the bulk of the gel or capillary pores. However, while the C-S-H unit cell does not exhibit well-defined pores that can be straightforwardly established by diffraction methods, it is considered that there is an interlayer space confining water similar to a clay with distances ranging from 2 to 4 Å[31–33]. Our data confirms[21] that in the case of the SCSA, the motion of the water molecules is within this interlayer distance, and that a number of hydrogen atoms bound in the to the C-S-H lattice can jump between two separated sites, but are not allowed to diffuse freely. Note that the jump distance, d, corresponds well to the distance between two neighboring H sites in H_2O. Finally, we conclude that the data presented here shows that in addition to the "pore blocking" theory of Bakker[5], it is the reaction of the blended pastes, which has promoted changes to the C-S-H structure so that it can interact more strongly with water molecules than the C-S-H structure of an OPC paste. As a result, there is a decrease of permeability water in the blended pastes.

Methods

Sample preparation details. See Supplementary Information for full preparation and characterization of the sugar cane straw ash and cement pastes.

Quasi-elastic neutron scattering. Neutron scattering spectra were measured using the ToF inverted geometry crystal analyser spectrometer IRIS[34] located at ISIS, UK. An elastic energy resolution, ΔE, of 17.5 μeV (at Full width at Half Maximum (FWHM)) was achieved by using the 002 analysing reflection of the pyrolytic graphite analyser crystals (PG002); the analyzer crystals Bragg reflecting only those neutrons scattered with λ = 6.7 Å This resolution was constant over the entire an angular scattering range; 25° < θ < 160° After being crushed by manual grinding, the cured samples were confined in an flat plate aluminium container and sealed inside an aluminium foil packet to avoid corrosion of the sample holder. The angle between the plane of the sample and the incident neutron beam was 135°. Using this orientation the last 8 high scattering angle detectors had to be discarded due to self-shielding from the edge of the sample can.

Additional details. Experimental procedure for the neutron scattering measurements, data reduction and analysis are provided in the supplementary information.

1. Dobbs, R. *et al*. Infrastructure productivity: how to save $1 trillion a year (McKinsey Global Institute, 2013).
2. Neville, A. M. Properties of Concrete (Prentice Hall, Inc, New Jersey, 1995).
3. Isaia, G. C., Gastaldini, A. L. G. & Moraes, R. Physical and pozzolanic action of mineral additions on the mechanical strength of high-performance concrete. *Cement and Concrete Composites* **25**, 69–76 (2003).

4. Sata, V., Tangpagasit, J., Jaturapitakkul, C. & Chindaprasirt, P. Effect of W/B ratios on pozzolanic reaction of biomass ashes in Portland cement matrix. *Cement and Concrete Composites* **34**, 94–100 (2012).

5. Bakker, R. F. M. SP-79 Proceedings of the 1st International Conference on the Use of Fly Ash, Slag and Silica Fume in Concrete Permeability of blended cement concretes (American Concrete Institute: Farmington Hills, 1983).

6. Phair, J. W. Green chemistry for sustainable cement production and use. *Green Chemistry* **8**, 763–780 (2006).

7. Amato, I. Green cement: concrete solutions. *Nature* **494**, 300–301 (2013).

8. Young, J. F. & Hansen, W. Microstructural Development during Hydration of Cement (Materials Research Society Symposium Proceedings, Boston Mass., USA, 1986).

9. Givi, A. N., Rashid, S. A., Aziz, F. N. A. & Salleh, M. A. M. Experimental investigation of the size effects of SiO_2 nano-particles on the mechanical properties of binary blended concrete. *Composites Part B: Engineering* **41**, 673–677 (2010).

10. Hooton, R. D. Blended Cements ASTM special technical publication 897. (American Society for Testing and Materials, USA, 1986).

11. Provis, J. L. & Deventer, J. S. J. V. Geopolymers: Structures, Processing, Properties and industrial Applications (CRC Press, 2009).

12. Schmidt, M., Middendorf, B., Vellmer, C. & Geisenhanslueke, C. Innovations in Portland Cement Manufacturing. (Portland Cement Association: Skokie, Illinois, 2004).

13. Frías, M., Villar, E. & Savastano, H. Brazilian sugar cane bagasse ashes from the cogeneration industry as active pozzolans for cement manufacture. *Cement and Concrete Composites* **33**, 490–496 (2011).

14. Martirena, F. *et al.* Rudimentary, low tech incinerators as a means to produce reactive pozzolan out of sugar cane straw. *Concrete and Concrete Research* **36**, 1056–1061 (2006).

15. Mindess, S., Young, J. F. & Darwin, D. Concrete (Prentice Hall, Inc, New Jersey, 2003).

16. Brubach, J.-B. *et al.* Dependence of water dynamics upon confinement size. *J. Phys. Chem B* **105**, 430–435 (2001).

17. Hartman, M. R. & Berliner, R. Investigation of the structure of ettringite by time-of-flight neutron powder diffraction techniques. *Cement and Concrete Research* **36**, 364–370 (2006).

18. Sakamoto, M., Brockhouse, B. N., Johnson, R. G. & Pope, N. K. Neutron inelastic scattering study of water. *J. Phys. Soc. Jpn.* **17**, Suppl. B II, 370 (1962).

19. Harris, D. H. C., Windsor, C. G. & Lawrence, C. D. Free and bound water in cement pastes. *Magazine of Concrete Research* **26**, 65–72 (1974).

20. Bordallo, H. N. & Aldridge, L. P. Concrete and cement paste studied by quasi-elastic neutron scattering. *Z. Phys. Chem.* **224**, 183–200 (2010).

21. Bordallo, H. N. *et al.* Hindered water motions in hardened cement pastes investigated over broad time and length scales. *ACS Applied Materials & Interfaces* **1**, 2154–2162 (2009).

22. Fratini, E., Ridi, F., Chen, S.-H. & Baglioni, P. Hydration water and microstructure in calcium silicate and aluminate hydrates. *Journal of Physics: Condensed Matter* **18**, S2467–S2483 (2006).

23. Bordallo, H. N., Aldridge, L. P. & Desmedt, A. Water dynamics in hardened ordinary portland cement paste or concrete: from quasielastic neutron scattering. *J. Phys. Chem B* **110**, 17966–17976 (2006).

24. Ridi, F., Luciani, P., Fratini, E. & Baglioni, P. Water confined in cement pastes as a probe of cement microstructure evolution. *J. Phys. Chem B* **113**, 3080–3087 (2009).

25. Peterson, V. K., Brown, C. M. & Livingston, R. A. Quasielastic and inelastic neutron scattering study of the hydration of monoclinic and triclinic tricalcium silicate. *Chemical Physics* **326**, 381–389 (2006).

26. Lovensy, S. W. Theory of Neutron Scattering from Condensed Matter (University Press, Oxford, 1984).

27. Gates, W. P., Bordallo, H. N., Aldridge, L. P., Seydel, T., Jacobsen, H., Marry, V. & Churchman, G. Jock Neutron time-of-flight quantification of water desorption isotherms of montmorillonite. *J. Phys. Chem C* **116**, 5558–5570 (2012).

28. Singwi, K. S. & Sjölander, A. Diffusive motions in water and cold neutron scattering. *Phys. Rev.* **119**, 863–871 (1960).

29. Volino, F. & Dianoux, A. J. Neutron incoherent scattering law for diffusion in a potential of spherical symmetry: general formalism and application to diffusion inside a sphere. *Molecular Physics* **41**, 271–279 (1980).

30. Bellissent-Funel, M. C., Teixeira, J., Bradley, K. & Chen, S. H. Dynamics of hydration water in protein. *J. Phys. I* **2**, 995–1001 (1992).

31. Ji, Q., Pellenq, R. J.-M. & Van Vliet, K. J. Comparison of computational water models for simulation of calcium–silicate–hydrate. *Computational Materials Science* **53**, 234–240 (2012).

32. Pellenq, R. J.-M. *et al.* A realistic molecular model of cement hydrates. *PNAS* **106**, 16102–16107 (2009).

33. Taylor, H. F. W. Cement Chemistry (Thomas Telford, London, 1997).

34. Carlile, C. J. & Adams, M. A. The design of the IRIS inelastic neutron spectrometer and improvements to its analyzers. *Physica B* **182**, 431–440 (1992).

Acknowledgments

Author contributions

H.N.B. conceived the project with input from M.S.R., L.P.A., A.L.B. and S.F.S. M.S.R. prepared and characterized the samples. H.N.B., M.T.F.T. and L.P.A. designed the experiments. H.N.B., M.T.F.T. and J.J. carried out the QENS experiment and analysed the data. H.N.B. wrote the paper, which was approved by all co-authors in its final version. J.J. and M.S.R. contributed equally.

Additional information